

## Picometer-Resolved Photoemission Position within the Molecule by Strong-Field Photoelectron Holography

Wenhai Xie<sup>1</sup>, Jiaqing Yan<sup>1</sup>, Min Li<sup>1,\*</sup>, Chuanpeng Cao<sup>1</sup>, Keyu Guo<sup>1</sup>, Yueming Zhou<sup>1</sup>, and Peixiang Lu<sup>1,2,3,†</sup>

<sup>1</sup>Wuhan National Laboratory for Optoelectronics and School of Physics, Huazhong University of Science and Technology, Wuhan 430074, China

<sup>2</sup>Hubei Key Laboratory of Optical Information and Pattern Recognition, Wuhan Institute of Technology, Wuhan 430205, China

<sup>3</sup>CAS Center for Excellence in Ultra-intense Laser Science, Shanghai 201800, China



(Received 17 June 2021; accepted 4 November 2021; published 22 December 2021)

Laser-induced tunneling ionization is one of the fundamental light-matter interaction processes. An accurate description of the tunnel-ionized electron wave packet is central to understanding and controlling subsequent electron dynamics. Because of the anisotropic molecular structure, tunneling ionization of molecules involves considerable challenges in accurately describing the tunneling electron wave packet. Up to now, some basic properties of the tunneling electron from molecules still remain unexplored. Here, we demonstrate that the tunneling electron from a molecule is not always emitted from the geometric center of the molecule along the tunnel direction. Rather, the photoemission position depends on the molecular orientation. Using a photoelectron holographic technique, we determine the photoemission position for a nitrogen molecule relative to the molecular geometric center to be  $95 \pm 21$  pm when the molecular axis is oriented along the tunnel direction. Our Letter poses, and answers experimentally, a fundamental question as to where the molecular photoionization actually begins, which has significant implications for time-resolved probing of valence electron dynamics in molecules.

DOI: 10.1103/PhysRevLett.127.263202

Tunneling ionization of atoms and molecules triggers a variety of strong-field processes, forming the basis for numerous emerging techniques to probe the dynamical behavior of matter on the attosecond timescale [1]. The property of the electron created by tunneling ionization critically determines the subsequent dynamics, hence an accurate description of the tunneling electron wave packet is of paramount importance for attosecond science. Previous experiments have investigated the exit position of the tunneling electron [2], the momentum distribution of the electron at the tunnel exit [3–7], the phase distribution of the tunneling electron wave packet [8,9], and the time when the electron exits the tunneling barrier [10,11]. Using an attoclock technique, the time needed for an electron to tunnel through a potential barrier is also measured, although this issue is still controversial [12–16]. Such information is essential to our understanding of many ultrafast phenomena that are often interpreted in terms of classical trajectories starting from the tunnel exit.

However, those measurements did not cover a basic question about the spatial position inside an atom or a molecule from which the tunneling electron wave packet emerged. As shown in Fig. 1(a), we take a  $N_2$  molecule as an example. When the molecular axis is oriented along the instantaneous tunnel direction, the highest occupied molecular orbital (HOMO) is elongated at this direction. Though the HOMO is symmetric with the molecular center, the instantaneous electric field of the laser breaks the spatial

symmetry, leading to a stronger interaction with the instantaneous laser field for the left-hand part of the wave function than the right-hand part. As a result, the tunneling electron might be emitted from an initial spatial coordinate of  $r_0$ , instead of the geometric center of the molecule. Notably, the expected photoemission position relative to the molecular geometric center is much smaller than the tunnel exit position  $r_e$ . Previous studies often neglected such small photoemission position and assumed that the electrons are emitted from the nuclei or the center of the molecule. This means that the characteristic spatial shape of the initial orbital was ignored in the tunneling ionization; e.g., the tunneling ionization of  $H_2^+$  and  $N_2$  molecules (both HOMOs are  $\sigma_g$  orbitals) was considered to be very similar, though the spatial shape of the HOMO is different [8,17].

The effect of the spatial distribution of electron probability density might lead to a nonvanishing photoemission position  $r_0$  relative to the molecular center, which will modify the electron motion under the potential barrier. From the perspective of the quantum-orbit theory [18–20], the electron takes an imaginary time under the potential barrier, which is closely related to the hotly discussed nonadiabatic effect of the tunneling ionization [5–7]. As shown in Fig. 1(a), this imaginary time  $t_i$  depends on the photoemission position, thus the photoemission position is crucial for quantifying the nonadiabaticity of the tunneling ionization. Moreover, the photoemission position has an impact on the phase of the electron accumulated along the

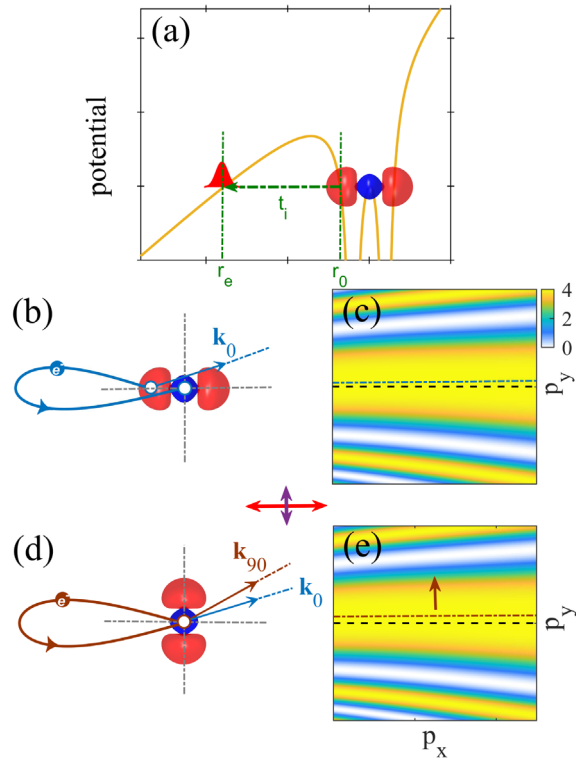


FIG. 1. (a) The schematic of tunneling ionization of a  $N_2$  molecule aligned along the tunnel direction. Because of the effect of the molecular orbital, the ionized electron wave packet might be emitted from an initial coordinate (photoemission position) of  $r_0$ , rather than the center of the molecule. (b)–(e) The scheme of probing the photoemission position with photoelectron holographic interferometry. By adding a weak 400-nm linearly polarized laser field perpendicular to the polarization direction of a strong 800-nm field, the rescattering electron will return to the molecular geometric center with different intermediate canonical momenta along the 400-nm-field direction depending on the photoemission position (b),(d). The intermediate canonical momentum will be mapped onto the shift of the holographic fringe along the 400-nm-field direction (c),(e). The holographic patterns are simulated by the strong-field approximation in (c) and (e), in which the dashed and dash-dotted lines show the central maxima of the holographic structures without and with the weak 400-nm field, respectively. The arrow in (e) shows the shift direction of the holographic fringes.

trajectory, and thus further affects the extraction of the Wigner time delay for the strong-field ionization of molecules [21] and the interpretation of the photoelectron interference in the photoelectron momentum distribution (PMD).

In this Letter, we measure such subtle photoemission positions of prealigned nitrogen molecules with a photoelectron holographic scheme, as outlined in Figs. 1(b)–1(e). The photoelectron holography is an ultrafast photoelectron spectroscopy, in which the interference of the direct and rescattering electron wave packets reveals a spiderlike structure in the PMD [22–30] (see a recent review in

Ref. [31]). In a strong 800-nm laser field, the photoelectron holographic pattern has a maximum along the field polarization direction, which corresponds to the central maximum of the hologram. By adding a weak 400-nm field perpendicular to the polarization of the strong 800-nm field, the holographic fringe becomes asymmetric in such an orthogonally polarized two-color (OTC) laser field, leading to a momentum shift of the central maximum along the 400-nm-field direction. This momentum shift depends on the photoemission position. In Fig. 1, we illustrate the relation between the momentum shift of the holographic fringe and the photoemission position. Released from a photoemission position  $r_0$ , the electron obtains an intermediate canonical momentum  $\mathbf{k}$  and then near-forward scatters off the molecular center. For a larger  $r_0$ , the electron takes a smaller imaginary time during the tunneling process and obtains a smaller intermediate canonical momentum along the 400-nm-field direction. This intermediate canonical momentum is mapped onto the shift of the holographic fringe [7,29]. Hence, inspecting the fringe shift in the OTC field offers a way to measure  $r_0$ .

We implemented this scheme using a similar experimental setup to that used in a previous experiment studying the molecular attoclock [32]. Briefly, the laser pulse was centered at 800 nm with a repetition rate of 5 kHz and a pulse duration of about 40 fs. It was split in a Michelson interferometer into an alignment pulse and a probe pulse with an adjustable delay. The duration of the alignment pulse was stretched to about 150 fs through a 12-mm-thick SF11 glass. The delay between the probe pulse and the alignment pulse was set to be  $\sim 8.33$  ps for  $N_2$  molecules to generate a macroscopic field-free alignment around the polarization axis of the alignment pulse [33]. The degree of alignment  $\langle \cos^2\theta \rangle$  is estimated to be  $\sim 0.65$ . The probe laser pulse was propagated through a 300- $\mu\text{m}$ -thick  $\beta$ -barium borate ( $\beta$ -BBO) crystal for second harmonic generation. After the BBO, the probe laser pulse became an OTC laser field. The polarization direction of the alignment laser beam was either along the 800-nm-field direction ( $x$  direction corresponding to  $\phi = 0^\circ$ ) or along the 400-nm-field direction ( $y$  direction corresponding to  $\phi = 90^\circ$ ) of the probe pulse. Each direction was maintained for  $\sim 20$  min by means of half-wave plate mounted on a computer-controlled rotary stage. The alignment and probe beams were recombined and focused by an  $f = 75$ -mm parabolic mirror into a  $N_2$  gas jet. The three-dimensional momenta of the resulting photoelectrons were detected using cold target recoil ion momentum spectroscopy [34,35]. The intensity of the 800- and 400-nm components of the OTC field was calibrated to be  $\sim 6.2 \times 10^{13}$  and  $\sim 1.2 \times 10^{12}$  W/cm $^2$ , respectively.

The measured PMDs in the OTC laser fields for  $N_2$  molecules with the alignment angles of  $\phi = 0^\circ$  and  $\phi = 90^\circ$  are shown in Figs. 2(a) and 2(b), respectively, which reveal that the holographic patterns are asymmetric with respect to

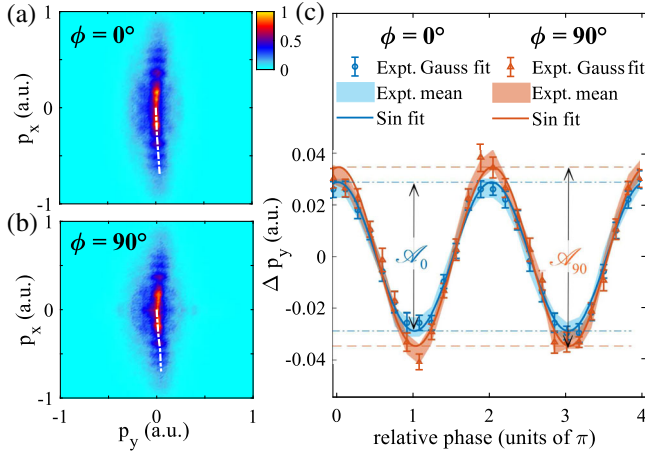


FIG. 2. (a),(b) The measured PMDs in the OTC laser fields of  $N_2$  molecules with alignment angles of (a)  $\phi = 0^\circ$  and (b)  $\phi = 90^\circ$ . The central maximum of the PMD is guided by the white dashed lines. The relative phase of the OTC fields is the same for (a) and (b), corresponding to the most asymmetric fringes for the holographic structures. (c) The shift  $\Delta p_y$  of the central maximum as a function of the relative phase for the alignment angles of  $\phi = 0^\circ$  and  $\phi = 90^\circ$  at  $p_x = 0.4$  a.u. The solid lines show the fitting results of the experimental data with a sinusoidal function.

$p_y = 0$  for both cases. The central maximum of the PMD is guided by the white dashed lines, which corresponds to zero scattering angle at the instant of rescattering for the electron. The Coulomb potential enhances the relative contribution of the rescattering electron with zero scattering angle owing to the large scattering cross section. As a result, the central maximum is very clear in the PMD and we will use the shift of the central maximum to extract the photoemission position. The shift of the central maximum depends on the relative phase of the OTC field. In Fig. 2(c), we show the comparison of the fringe shift for  $\phi = 0^\circ$  with that for  $\phi = 90^\circ$  at  $p_x = 0.4$  a.u. as a function of the relative phase of the OTC field. Atomic units are used unless specified otherwise. The shift of the central maximum from the measurement can be obtained either from a Gaussian fitting process or from the mean value of the  $p_y$  momentum distribution. One can see that the fringe shifts are nearly the same using those two methods. The solid curves in Fig. 2(c) show a sinusoidal function fitting of the oscillation of the fringe shift. It is clear that the amplitude of the oscillation for  $\phi = 90^\circ$  ( $\mathcal{A}_{90}$ ) is larger than that for  $\phi = 0^\circ$  ( $\mathcal{A}_0$ ).

The amplitude  $\mathcal{A}$  of the oscillation of the fringe shift as a function of the final momentum  $p_x$  is shown in Fig. 3(a) for  $\phi = 0^\circ$  and  $\phi = 90^\circ$ , which reveals that the amplitude  $\mathcal{A}$  of  $\phi = 90^\circ$  is larger than that of  $\phi = 0^\circ$  for all  $p_x$ . Theoretically, the fringe shift of the holographic pattern is determined by the phase difference between the rescattering and direct electron wave packets. In the OTC field, the phase difference can be written as [7,29]

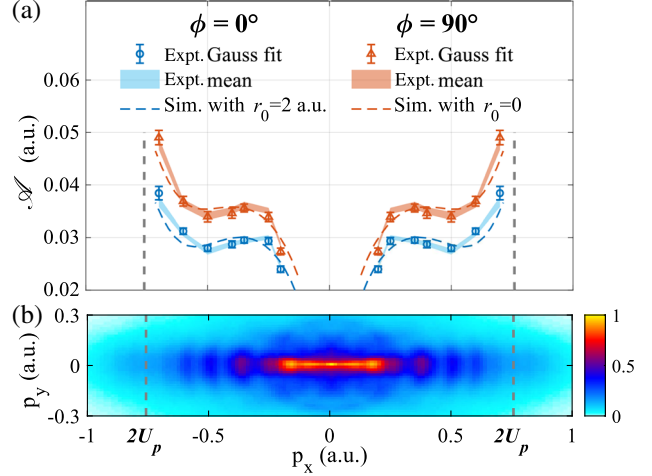


FIG. 3. (a)  $\mathcal{A}$  with respect to the final momentum  $p_x$ , where  $\mathcal{A}$  is the amplitude of the oscillation of the fringe shift with the relative phase. For comparison, the simulated results with assuming an initial photoemission position of  $r_0 = 2$  a.u. and  $r_0 = 0$  are shown by the dashed blue and red curves, respectively. (b) The PMD in a single 800-nm laser field. The vertical dashed lines show the position of the classical  $2U_p$  cutoff.

$$\Delta S \approx \frac{(p_y - k_y)^2}{2} (t_c - t_0) + \alpha, \quad (1)$$

where  $\mathbf{k} = -[1/(t_c - t_s)] \int_{t_s}^{t_c} \mathbf{A}(\tau) d\tau$  is the intermediate canonical momentum of the rescattering electron,  $\mathbf{A}(\tau)$  is the laser vector potential,  $t_s$  is the saddle-point time,  $t_c$  is the rescattering time,  $t_0$  is the ionization time, and  $\alpha$  is the phase arising from the interaction between the electron and the parent ion. The subscript  $y$  indicates the weak 400-nm-field direction. Comparing Eq. (1) with the phase difference in a single-color laser field, i.e.,  $\Delta S \approx (p_y^2/2)(t_c - t_0) + \alpha$ , we know that the shift of the central maximum with respect to  $p_y = 0$  is the intermediate canonical momentum  $k_y$  in the OTC field [7,29].

Using the molecular strong-field approximation [36–38], the intermediate canonical momentum  $k_y$  can be obtained from the saddle-point equation for the rescattering electron (see Supplemental Material for details [39]),

$$[\mathbf{k} + \mathbf{A}(t_s)]^2/2 + I_p - s\mathbf{E}(t_s) \cdot \mathbf{r}_0 = 0, \quad (2a)$$

$$(t_s - t_c)\mathbf{k} = \int_{t_s}^{t_c} \mathbf{A}(t) dt - s\mathbf{r}_0, \quad (2b)$$

$$[\mathbf{k} + \mathbf{A}(t_c)]^2/2 = [\mathbf{p} + \mathbf{A}(t_c)]^2/2, \quad (2c)$$

where  $I_p$  is the ionization potential,  $\mathbf{E}$  is the laser electric field, and  $s = 1$  for the electron emitted from the left side of the molecular wave function and  $s = -1$  from the right side. Equations 2(a) and 2(c) stand for the energy conservation at the moment of ionization and rescattering, respectively, and Eq. 2(b) stands for the return condition for the rescattering

electron. Compared to the case of atoms, Eq. 2(a) includes an additional potential energy term  $-s\mathbf{E}(t_s) \cdot \mathbf{r}_0$ . This term defines the energy gain or loss for the electron to travel from the position of  $-s\mathbf{r}_0$  to the molecular center, which means that the electron is released from the position of  $-s\mathbf{r}_0$ . For the return condition, there is also an additional term  $-s\mathbf{r}_0$  on the right-hand side of Eq. (2b), indicating that the electron is released from  $-s\mathbf{r}_0$  and then scatters at the molecular center. Therefore, the photoemission position  $r_0$  has been included in the saddle-point equation and has an influence on the fringe shift, i.e.,  $k_y$ .

To extract the photoemission position from the fringe shift, we numerically solve the saddle-point equation (2) to obtain the quantitative relation between the fringe shift and the photoemission position  $r_0$ . Because the photoionization for  $\phi = 90^\circ$  is similar to the case of an atom, the photoemission position for  $\phi = 90^\circ$  is nearly zero. Therefore, we minimize systematic errors by taking the case of  $\phi = 90^\circ$  as a reference. We denote the difference of the amplitude between  $\phi = 0^\circ$  and  $\phi = 90^\circ$  as  $\Delta\mathcal{A} \equiv \mathcal{A}_0 - \mathcal{A}_{90}$ . By numerically solving the saddle-point equation (2), we find that  $\Delta\mathcal{A}$  is directly proportional to the photoemission position [39], i.e.,

$$\Delta\mathcal{A} \approx f(p_x)r_0, \quad (3)$$

where  $f(p_x)$  is a coefficient determined by solving Eq. (2). Equation (3) allows us to directly extract the photoemission position  $r_0$  from the measured  $\Delta\mathcal{A}$ . Note that we did not consider the effect of the bound excited states in Eq. (3). The effect of the excited states is negligible in the momentum range of  $[0.2, 0.7]$  a.u. because the phase of the released electron wave packet is affected by the excited states only at near-vanishing field strength [43].

The extracted photoemission position is shown in Fig. 4(a) for  $\phi = 0^\circ$ , which is nearly independent on the final electron momentum  $p_x$ . By taking the averaged result at different  $p_x$ , we determine the photoemission position relative to the molecular center to be  $1.8 \pm 0.4$  a.u., corresponding to  $95 \pm 21$  pm. For comparison, we also show the nuclei position relative to the molecular center ( $R_0/2 = 1.03$  a.u. where  $R_0$  is the internuclear separation) by the dashed line, which is significantly smaller than the extracted  $r_0$ . This deviation can be understood by approximately considering the HOMO of the molecule as a linear combination of atomic orbitals. When the HOMO of a molecule is only contributed by the atomic  $s$  orbitals, the tunneling electron is released from the nucleus. However, for a  $\text{N}_2$  molecule, the atomic  $p$  orbital has a significant contribution to its HOMO [36]. Compared to the  $s$  orbital, the maximum of the probability amplitude of the  $p$  orbital deviates from the nuclear position, leading to a larger tunneling ionization rate for the part of the orbital opposite to the instantaneous laser-field direction than the part along the laser-field direction. As a result, the center of the

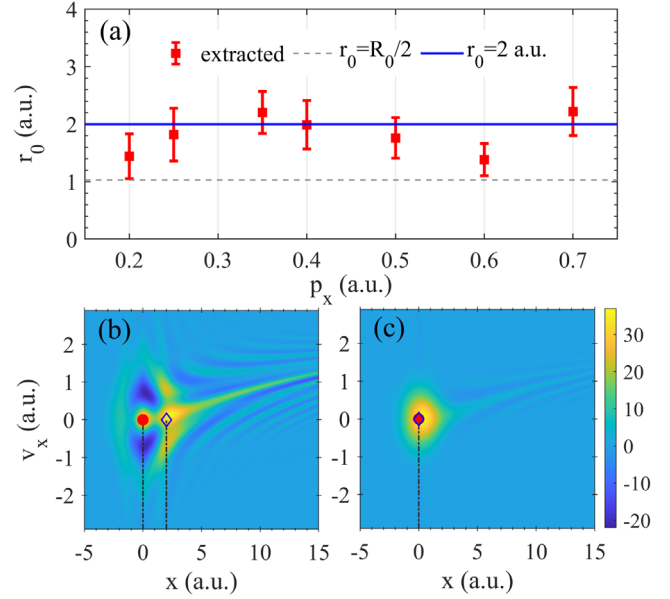


FIG. 4. (a) The extracted photoemission position of  $\text{N}_2$  molecules for the alignment angle of  $\phi = 0^\circ$ . The nuclear position relative to the molecular center ( $R_0/2$ ) is shown by the dashed line, and the most probable photoemission position from the Wigner function distribution is shown by the blue solid line. (b), (c) The Wigner function distributions for the  $\text{N}_2$  molecules with alignment angles of (b)  $\phi = 0^\circ$  and (c)  $\phi = 90^\circ$ . The red dots and blue rhombi show the molecular geometric centers and the most probable photoemission positions, respectively.

released electron wave packet does not correspond to the nuclei position.

To validate our result, we further determine the photoemission position from the Wigner function distribution. The Wigner function employs the classical concept of phase space in quantum theory, which has been used to identify the difference between the Wigner tunneling trajectory and the classical trajectory [44,45]. For an electron in a state  $\tilde{\Psi}(v_x, t)$ , the Wigner function is given by  $W(v_x, x; t) = 1/\pi \int dp \tilde{\Psi}^*(v_x + p, t) e^{-2ixp} \tilde{\Psi}(v_x - p, t)$  with the position  $x$  and the momentum  $v_x$ . Within the strong-field approximation, the electron wave function in the momentum space reads  $\tilde{\Psi}(v_x, t) = -i \int_0^t \langle v_x + F(t-t') | x F | \Psi_{\text{mol}} \rangle \times e^{-i \int_{t'}^t [v_x + F(t-t'')]^2 / 2 dt''} e^{i I_p t'} dt' + \langle v_x | e^{i I_p t} | \Psi_{\text{mol}} \rangle$  [19,46], where  $|\Psi_{\text{mol}}\rangle$  is the initial wave function of the molecule and  $F = 0.1$  a.u. is the strength of a static electric field. The Wigner functions  $W(v_x, x; t \rightarrow \infty)$  clearly show the trajectory of the electron probability current from the photoemission position to the continuum, as shown in Figs. 4(b) and 4(c), corresponding to  $\phi = 0^\circ$  and  $\phi = 90^\circ$ , respectively. The photoemission position obviously depends on the molecular orientation, which is nearly zero for  $\phi = 90^\circ$  and becomes  $\sim 2$  a.u. for  $\phi = 0^\circ$ . The latter is in a good agreement with the extracted one from the measurement ( $1.8 \pm 0.4$  a.u.). With assuming a photoemission position of  $r_0 = 2$  a.u. ( $r_0 = 0$ )

when solving Eq. (2), we obtain the amplitude  $\mathcal{A}$  as a function of  $p_x$ , which agrees with the measurement for  $\phi = 0^\circ$  ( $\phi = 90^\circ$ ), as shown in Fig. 3(a). The extracted  $r_0$  is slightly smaller than the prediction of the Wigner function distribution, which comes from the assumption of perfect alignment of the molecules in the extraction procedure (see Supplemental Material [39]).

In conclusion, we have determined the photoemission position of prealigned nitrogen molecules with a photoelectron holographic interferometry. We for the first time demonstrate that picometer-resolved spatial information can be experimentally extracted using the strong-field photoelectron holography technique, thus paving the way toward monitoring charge migration in molecules [28]. The extracted photoemission position deviates from the nuclei position of the molecule and agrees well with the prediction of the Wigner function distributions. This finding provides new physical insight into how molecules are ionized in strong laser fields and has implications for laser-induced tunnel ionization in all molecules. Furthermore, the photoemission position will affect the phase of the electron accumulated along the trajectory, which is relevant to the timing of photoionization. Thus, our Letter also has significant implications for any attosecond metrology that is based on tunneling ionization, such as attoclock or high harmonic spectroscopy.

This work is supported by National Key Research and Development Program of China (Grant No. 2019YFA0308300) and National Natural Science Foundation of China (Grants No. 61475055 and No. 12021004).

W. X. and J. Y. contributed equally to this work.

\*mli@hust.edu.cn

†lupeixiang@hust.edu.cn

- [1] F. Krausz and M. Ivanov, *Rev. Mod. Phys.* **81**, 163 (2009).
- [2] A. N. Pfeiffer, C. Cirelli, M. Smolarski, D. Dimitrovski, M. Abusamha, L. B. Madsen, and U. Keller, *Nat. Phys.* **8**, 76 (2012).
- [3] L. Arissian, C. Smeenk, F. Turner, C. Trallero, A. V. Sokolov, D. M. Villeneuve, A. Staudte, and P. B. Corkum, *Phys. Rev. Lett.* **105**, 133002 (2010).
- [4] A. N. Pfeiffer, C. Cirelli, A. S. Landsman, M. Smolarski, D. Dimitrovski, L. B. Madsen, and U. Keller, *Phys. Rev. Lett.* **109**, 083002 (2012).
- [5] S. Eckart, K. Fehre, N. Eicke, A. Hartung, J. Rist, D. Trabert, N. Strenger, A. Pier, L. Ph. H. Schmidt, T. Jahnke, M. S. Schöffler, M. Lein, M. Kunitski, and R. Dörner, *Phys. Rev. Lett.* **121**, 163202 (2018).
- [6] K. Liu, S. Luo, M. Li, Y. Li, Y. Feng, B. Du, Y. Zhou, P. Lu, and I. Barth, *Phys. Rev. Lett.* **122**, 053202 (2019).
- [7] M. Li, H. Xie, W. Cao, S. Luo, J. Tan, Y. Feng, B. Du, W. Zhang, Y. Li, Q. Zhang, P. Lan, Y. Zhou, and P. Lu, *Phys. Rev. Lett.* **122**, 183202 (2019).
- [8] M. Meckel, A. Staudte, S. Patchkovskii, D. M. Villeneuve, P. B. Corkum, R. Dörner, and M. Spanner, *Nat. Phys.* **10**, 594 (2014).
- [9] M. Han, P. Ge, Y. Shao, M. M. Liu, Y. Deng, C. Wu, Q. Gong, and Y. Liu, *Phys. Rev. Lett.* **119**, 073201 (2017).
- [10] D. Shafir, H. Soifer, B. D. Bruner, M. Dagan, Y. Mairesse, S. Patchkovskii, M. Y. Ivanov, O. Smirnova, and N. Dudovich, *Nature (London)* **485**, 343 (2012).
- [11] G. Porat, G. Alon, S. Rozen, O. Pedatzur, M. Krüger, D. Azoury, A. Natan, G. Orenstein, B. D. Bruner, M. J. J. Vrakking, and N. Dudovich, *Nat. Commun.* **9**, 2805 (2018).
- [12] P. Eckle, A. N. Pfeiffer, C. Cirelli, A. Staudte, R. Dörner, H. G. Muller, M. Büttiker, and U. Keller, *Science* **322**, 1525 (2008).
- [13] A. S. Landsman, M. Weger, J. Maurer, R. Boge, A. Ludwig, S. Heuser, C. Cirelli, L. Gallmann, and U. Keller, *Optica* **1**, 343 (2014).
- [14] N. Camus, E. Yakaboylu, L. Fechner, M. Klaiber, M. Laux, Y. Mi, K. Z. Hatsagortsyan, T. Pfeifer, C. H. Keitel, and R. Moshhammer, *Phys. Rev. Lett.* **119**, 023201 (2017).
- [15] U. Sainadh, H. Xu, X. Wang, A. Atia-Tul-Noor, W. Wallace, N. Douguet, A. Bray, I. Ivanov, K. Bartschat, A. Kheifets, R. Sang, and I. Litvinyuk, *Nature (London)* **568**, 75 (2019).
- [16] W. Quan, V. V. Serov, M. Z. Wei, M. Zhao, Y. Zhou, Y. L. Wang, X. Y. Lai, A. S. Kheifets, and X. J. Liu, *Phys. Rev. Lett.* **123**, 223204 (2019).
- [17] M.-M. Liu, M. Li, C. Wu, Q. Gong, A. Staudte, and Y. Liu, *Phys. Rev. Lett.* **116**, 163004 (2016).
- [18] W. Becker, F. Grasbon, R. Kopold, D. B. Milošević, G. G. Paulus, and H. Walther, *Adv. At. Mol. Opt. Phys.* **48**, 35 (2002).
- [19] D. B. Milošević, G. G. Paulus, D. Bauer, and W. Becker, *J. Phys. B* **39**, R203 (2006).
- [20] V. S. Popov, *Phys. At. Nucl.* **68**, 686 (2005).
- [21] D. Trabert, S. Brennecke, K. Fehre, N. Anders, A. Geyer, S. Grundmann, M. S. Schöffler, L. Ph. H. Schmidt, T. Jahnke, R. Dörner, M. Kunitski, and S. Eckart, *Nat. Commun.* **12**, 1697 (2021).
- [22] Y. Huismans *et al.*, *Science* **331**, 61 (2011).
- [23] X. B. Bian, Y. Huismans, O. Smirnova, K. J. Yuan, M. J. J. Vrakking, and A. D. Bandrauk, *Phys. Rev. A* **84**, 043420 (2011).
- [24] X. B. Bian and A. D. Bandrauk, *Phys. Rev. Lett.* **108**, 263003 (2012).
- [25] M. Haertelt, X.-B. Bian, M. Spanner, A. Staudte, and P. B. Corkum, *Phys. Rev. Lett.* **116**, 133001 (2016).
- [26] Y. Zhou, O. I. Tolstikhin, and T. Morishita, *Phys. Rev. Lett.* **116**, 173001 (2016).
- [27] S. G. Walt, N. B. Ram, M. Atala, N. I. Shvetsov-Shilovski, A. von Conta, D. Baykusheva, M. Lein, and H. J. Wörner, *Nat. Commun.* **8**, 15651 (2017).
- [28] M. He, Y. Li, Y. Zhou, M. Li, W. Cao, and P. Lu, *Phys. Rev. Lett.* **120**, 133204 (2018).
- [29] J. Tan, Y. Zhou, M. He, Y. Chen, Q. Ke, J. Liang, X. Zhu, M. Li, and P. Lu, *Phys. Rev. Lett.* **121**, 253203 (2018).
- [30] Q. Z. Xia, J. F. Tao, J. Cai, L. B. Fu, and J. Liu, *Phys. Rev. Lett.* **121**, 143201 (2018); J. F. Tao, J. Cai, Q. Z. Xia, and J. Liu, *Phys. Rev. A* **101**, 043416 (2020).
- [31] C. Figueira de Morisson Faria and A. S. Maxwell, *Rep. Prog. Phys.* **83**, 034401 (2020).

- [32] J. Yan, W. Xie, M. Li, K. Liu, S. Luo, C. Cao, K. Guo, W. Cao, P. Lan, Q. Zhang, Y. Zhou, and P. Lu, *Phys. Rev. A* **102**, 013117 (2020).
- [33] D. Pavičić, K. F. Lee, D. M. Rayner, P. B. Corkum, and D. M. Villeneuve, *Phys. Rev. Lett.* **98**, 243001 (2007).
- [34] R. Dörner, V. Mergel, O. Jagutzki, L. Spielberger, J. Ullrich, R. Moshhammer, and H. Schmidt-Böcking, *Phys. Rep.* **330**, 95 (2000).
- [35] J. Ullrich, R. Moshhammer, A. Dorn, R. Dörner, L. Ph. H. Schmidt, and H. Schmidt-Böcking, *Rep. Prog. Phys.* **66**, 1463 (2003).
- [36] D. B. Milošević, *Phys. Rev. A* **74**, 063404 (2006).
- [37] O. Smirnova, M. Spanner, and M. Y. Ivanov, *J. Mod. Opt.* **54**, 1019 (2007).
- [38] A. Staudte, S. Patchkovskii, D. Pavičić, H. Akagi, O. Smirnova, D. Zeidler, M. Meckel, D. M. Villeneuve, R. Dörner, M. Y. Ivanov, and P. B. Corkum, *Phys. Rev. Lett.* **102**, 033004 (2009).
- [39] See Supplemental Material at <http://link.aps.org/supplemental/10.1103/PhysRevLett.127.263202> for details of the molecular strong-field approximation and the reconstruction procedure of the photoemission position, which includes Refs. [40–42].
- [40] P. E. Cade and A. C. Wahl, *At. Data Nucl. Data Tables* **13**, 339 (1974).
- [41] V. V. Serov, A. W. Bray, and A. S. Kheifets, *Phys. Rev. A* **99**, 063428 (2019).
- [42] X. M. Tong, Z. X. Zhao, and C. D. Lin, *Phys. Rev. A* **66**, 033402 (2002).
- [43] X. Xie, S. Roither, D. Kartashov, E. Persson, D. G. Arbó, L. Zhang, S. Gräfe, M. S. Schöffler, J. Burgdörfer, A. Baltuška, and M. Kitzler, *Phys. Rev. Lett.* **108**, 193004 (2012).
- [44] A. Czirják, R. Kopold, W. Becker, M. Kleber, and W. P. Schleich, *Opt. Commun.* **179**, 29 (2000).
- [45] M. Han, P. Ge, Y. Fang, X. Yu, Z. Guo, X. Ma, Y. Deng, Q. Gong, and Y. Liu, *Phys. Rev. Lett.* **123**, 073201 (2019).
- [46] M. Y. Ivanov, M. Spanner, and O. Smirnova, *J. Mod. Opt.* **52**, 165 (2005).